Progress of Theoretical Physics, Vol. 96, No. 5, November 1996

Relativistic Roche-Riemann Problems around a Black Hole

Masaru SHIBATA

Department of Earth and Space Science, Graduate School of Science
Osaka University, Toyonaka 560

(Received July 22, 1996)

Based on a framework of the hydrodynamics for a fluid star of mass m orbiting a Kerr black hole of mass $M \gg m$, relativistic Roche-Riemann ellipsoids for incompressible fluids are considered. It is found that in the relativistic Roche-Riemann limit for the irrotational Roche-Riemann ellipsoid moving at the innermost stable circular orbit around Kerr black holes, the angular velocity, Ω, becomes $\Omega^2 \simeq 0.063637\pi\rho$. We also argue implications of present results on the final fate of black hole-neutron star binary systems.

§ 1. Introduction

The final fate of close binary systems of stellar mass black hole (BH) and neutron star (NS) is taken interest from two reasons. One is that they are regarded as one of the most promising sources for kilo-meter-size laser interferometric gravitational wave detector such as LIGO.[1] When the binary is close enough, gravitational waves from them will be detected up to the tidal disruption of the NS or the plunging of the NS into the BH. In particular, gravitational waves from the final phase will bring us a wide variety of information about a highly relativistic phenomenon. The other reason is that BH-NS binaries are proposed as one of the likely candidates for γ-ray burst sources.[2] A scenario suggests that if the NS is tidally disrupted before plunging into the BH, some of the matter will form a disk around the BH, which releases a sufficient energy to produce the γ- ray bursts. A key assumption in this scenario is that the NS is tidally disrupted by the BH before coalescence to be the accretion disk around the BH. Thus, in either point of view, it is necessary to clarify the final fate of the BH-NS binary systems.

To investigate the dynamical evolution of BH-NS binaries just before the coalescence accurately, we need a fully general relativistic simulation, but it is a very difficult problem. Hence, in this paper, we simplify the problem imposing the following assumptions in analysis;

(1) we assume that the mass of NSs is sufficiently smaller than that of BHs and that the center of mass of a NS moves along the geodesic in the BH spacetime.

(2) the radius of the NS is assumed to be much larger than its Schwarzschild radius, and we use the Newtonian hydrodynamic equations for describing internal structure of the NS.

(3) we assume that the radius of the NS is much smaller than the background curvature of the BH spacetime; this implies that the external tidal forces can be evaluated by the tidal tensor obtained by Fishbone,[3] Mashhoon[4] and Marck,[5] in which the tidal tensor field is derived from the geodesic deviation equation by

analogy.

Thus, the general relativistic effects are taken into account only in the orbit and tidal tensor on the NS orbiting a BH. Since the general relativity plays an important role to determine the internal structure of NSs and also the gravity from the NS affects the orbital motion of BH-NS binaries, analysis performed under these assumptions is a very rough one. However, it will bring us a guideline to this problem. More accurate analysis must be done in future works.

The paper is organized as follows: In § 2, we review the hydrodynamic formulation for the fluid moving around a Kerr BH which has been developed previously.[3)~5)] In § 3, we present equilibrium configurations of relativistic Roche-Riemann ellipsoids. Numerical results for a relativistic Roche problem were shown by Fishbone previously.[3)] Here, we include the internal motion of the fluid to consider Roche-Riemann sequences which are likely realized in BH-NS binaries.[6)] We show the Roche-Riemann limit*) for various sets of orbital radius and spin parameter of Kerr BH. In § 4, we investigate the stability (i.e., tidal disruption point) of the Roche-Riemann ellipsoid near the Roche-Riemann limit performing the time evolution of the dynamical equations. We will show that for the irrotational Roche-Riemann ellipsoid (IRRE), the point where the dynamical instability sets in approximately coincides with the Roche-Riemann limit. We discuss implications of results obtained in §§ 3 and 4 on the final fate of BH-NS binaries in § 5. Hereafter, we use the units $c=G=1$.

§ 2. Formulation

A formalism of the hydrodynamics for a fluid star orbiting a Kerr BH has been developed by Fishbone,[3)] Mashhoon[4)] and Marck.[5)] In their formalism, they consider a self-gravitating fluid star of mass m and characteristic radius $R \gg m$. Assuming that the mass of the BH, M, is much larger than m, the trajectory of the star is chosen as a geodesic around the Kerr BH characterized by three constants of motion (E, L, C), where E, L and C denote the energy, the angular momentum of z-component and the Carter constant. Since the background curvature scale ($\geq M$) is assumed to be much larger than R, the tidal field by the BH to the fluid star is derived from the geodesic deviation equation. In this paper, we consider the hydrodynamics of the fluid star in the equatorial plane of a Kerr BH (i.e., $C=0$). In this case, equations of motion for a self-gravitating fluid star orbiting a Kerr BH of mass $M \gg m$ and spin a is as follows:

$$\rho \frac{du_i}{d\tau} = -\frac{\partial P}{\partial X_i} - \rho \frac{\partial \phi}{\partial X_i} - \rho \sum_{j=1}^{3} C_{ij} X_j , \tag{2·1}$$

where τ is the affine parameter of the geodesic, X_i is the coordinates chosen to be orthogonal to the geodesic, u_i is the velocity of the internal motion of the fluid, ρ is the density, P is the pressure, and ϕ is the Newtonian potential which obeys

*) Here, the Roche-Riemann limit is defined as the place along a Roche-Riemann sequence where a star of certain density orbiting a BH has the maximum orbital angular frequency (or the minimum orbital radius). This implies that inside this radius, no equilibrium state of the star is possible, but this does not always imply that the star is disrupted there.

$$\Delta\phi=4\pi\rho\,. \tag{2·2}$$

$C_{ij}=C_{ji}$ is the tidal tensor, defined as

$$C_{11}=\frac{M}{r^3}\left(1-3\frac{r^2+K}{r^2}\cos^2\Psi\right), \tag{2·3}$$

$$C_{22}=\frac{M}{r^3}\left(1-3\frac{r^2+K}{r^2}\sin^2\Psi\right), \tag{2·4}$$

$$C_{33}=\frac{M}{r^3}\left(1+3\frac{K}{r^2}\right), \tag{2·5}$$

$$C_{12}=C_{21}=-3\frac{M}{r^3}\frac{r^2+K}{r^2}\cos\Psi\sin\Psi\,, \tag{2·6}$$

$$C_{13}=C_{31}=C_{23}=C_{32}=0\,, \tag{2·7}$$

where "1", "2" and "3" components denote the axes of an orthonormal tetrad which is parallel-propagated along the geodesic, and they are chosen as follows;[5),*)] the 0-axis is chosen to be tangent to the geodesic; the 3-axis is determined to be perpendicular to the equatorial plane (i.e., parallel to the z-axis), and the 1- and 2-axes are perpendicular to the 3-axis. In the Newtonian limit ($r\gg M$), the 1- and 2-axes are in the equatorial plane. r is the radial coordinate in the Boyer-Lindquist coordinates, and K denotes $(L-aE)^2$. (Note that the Newtonian limit can be taken by setting $K=0$.) Ψ is a rotation angle and obeys the following equation,[5)]

$$\dot{\Psi}=\frac{(L-aE)E+a}{r^2+K}\equiv S_\Psi\,, \tag{2·8}$$

where "$\cdot$" denotes $\partial/\partial\tau$. In the case of a circular orbit at $r=r_0$, E, L, K and S_Ψ become

$$E=\frac{r_0^{3/2}-2Mr_0^{1/2}+aM^{1/2}}{r_0^{1/2}P_0^{1/2}}, \tag{2·9}$$

$$L=\frac{M^{1/2}(r_0^2-2aM^{1/2}r_0^{1/2}+a^2)}{r_0^{1/2}P_0^{1/2}}, \tag{2·10}$$

$$K=r_0^2\left(\frac{\Delta_0}{P_0}-1\right), \tag{2·11}$$

$$S_\Psi=\sqrt{\frac{M}{r_0^3}}\,, \tag{2·12}$$

where $P_0=r_0^2-3Mr_0+2aM^{1/2}r_0^{1/2}$ and $\Delta_0=r_0^2-2Mr_0+a^2$. Note that at the innermost stable circular orbit (ISCO), where $dE/dr_0=dL/dr_0=0$, Δ_0/P_0 is equal to 4/3 irrespective of spin parameter a.[3)]

Following Chandrasekhar[7)] and Mashhoon,[4)] we perform the coordinate transformation from the tetrad frame to a rotating frame as

*) Note that 2- and 3-axes chosen in this paper are those defined as 3- and 2-axes in Ref. 5).

$$x_i=\sum_{j=1}^{3} T_{ij}X_j\,, \tag{2·13}$$

where x_i denotes the coordinates in the rotating frame, and T_{ij} is the matrix which represents the orthogonal transformation,

$$\sum_{j=1}^{3} T_{ij}T_{jk}^{\dagger}=\delta_{ik}\,. \tag{2·14}$$

Here, $T_{jk}^{\dagger}$ is the transpose of T_{jk} (i.e., T_{kj}). In the following, we only consider the rotation around the 3-axis. Hence, we explicitly write T_{ij} as

$$T_{ij}=\begin{pmatrix} \cos\alpha & \sin\alpha & 0 \\ -\sin\alpha & \cos\alpha & 0 \\ 0 & 0 & 1 \end{pmatrix}, \tag{2·15}$$

where α is an argument and we define $\dot{\alpha}$ as Ω.

Then, we consider relativistic Roche-Riemann problems for incompressible fluids.[3] In this problem, ρ satisfies

$$\rho=\begin{cases} \rho_0=\text{const} & x_1^2/a_1^2+x_2^2/a_2^2+x_3^2/a_3^2\leq 1\,, \\ 0 & \text{otherwise}\,, \end{cases} \tag{2·16}$$

where $a_1(\tau)$, $a_2(\tau)$ and $a_3(\tau)$ are semi-axes, and they satisfy $(a_1a_2a_3)^{1/2}\equiv R_0=\{3m/(4\pi\rho_0)\}^{1/3}=\text{constant}$. Then, inside the fluid star, P and ϕ are written as

$$P=P_c\left(1-\sum_{i=1}^{3}\frac{x_i^2}{a_i^2}\right), \tag{2·17}$$

$$\phi=-\pi\rho\left(A_0-\sum_{i=1}^{3}A_ix_i^2\right), \tag{2·18}$$

where

$$A_i=a_1a_2a_3\int_0^{\infty}\frac{du}{D(a_i^2+u)}\,;\quad D(u)^2=(a_1^2+u)(a_2^2+u)(a_3^2+u)\,, \tag{2·19}$$

and $A_0=\sum_i a_i^2A_i$.[7]

Next, we define the vector $\tilde{x}_i=x_i/a_i$. The ellipsoidal shape of the fluid star does not change under the transformation $\tilde{x}_i=\sum_j S_{ij}(\tau)\tilde{x}_j(0)$ if S_{ij} is an orthogonal matrix, i.e., $\sum_j S_{ij}S_{jk}^{\dagger}=\delta_{ik}$.[7] This implies that the fluid star can have another degree of freedom for the internal motion, vorticity. Since we consider the vorticity only around the 3-axis in the following, we set S_{ij} as

$$S_{ij}=\begin{pmatrix} \cos\beta & \sin\beta & 0 \\ -\sin\beta & \cos\beta & 0 \\ 0 & 0 & 1 \end{pmatrix}, \tag{2·20}$$

where β is a variable and we define $\Lambda\equiv\dot{\beta}$.

Equations of motion for a_i, Ω and Λ become as follows:[4]

$$\ddot{a}_1=a_1(\Omega^2+\Lambda^2)-2a_2\Omega\Lambda-2\pi\rho_0 a_1 A_1+\frac{2P_c}{\rho_0 a_1}-\tilde{C}_{11}a_1\,, \tag{2·21}$$

$$\ddot{a}_2=a_2(\Omega^2+\Lambda^2)-2a_1\Omega\Lambda-2\pi\rho_0 a_2 A_2+\frac{2P_c}{\rho_0 a_2}-\tilde{C}_{22}a_2\,, \tag{2·22}$$

$$\ddot{a}_3=-2\pi\rho_0 a_3 A_3+\frac{2P_c}{\rho_0 a_3}-\tilde{C}_{33}a_3\,, \tag{2·23}$$

$$\dot{b}_1=-\dot{a}_1\Lambda+\dot{a}_2\Omega-\tilde{C}_{12}a_2\,, \tag{2·24}$$

$$\dot{b}_2=\dot{a}_2\Lambda-\dot{a}_1\Omega-\tilde{C}_{21}a_1\,, \tag{2·25}$$

where $\tilde{C}_{ij}=\sum_{k,l}T_{ik}C_{kl}T^{\dagger}_{lj}$, and

$$b_1=a_1\Lambda-a_2\Omega\,, \tag{2·26}$$

$$b_2=-a_2\Lambda+a_1\Omega\,. \tag{2·27}$$

Explicit forms of non-zero components for $\tilde{C}_{ij}$ are

$$\tilde{C}_{11}=\frac{M}{r^3}\left\{1-3\frac{r^2+K}{r^2}\cos^2(\Psi-\alpha)\right\}, \tag{2·28}$$

$$\tilde{C}_{22}=\frac{M}{r^3}\left\{1-3\frac{r^2+K}{r^2}\sin^2(\Psi-\alpha)\right\}, \tag{2·29}$$

$$\tilde{C}_{33}=\frac{M}{r^3}\left(1+3\frac{K}{r^2}\right), \tag{2·30}$$

$$\tilde{C}_{12}=\tilde{C}_{21}=-3\frac{M}{r^3}\frac{r^2+K}{r^2}\sin(\Psi-\alpha)\cos(\Psi-\alpha)\,. \tag{2·31}$$

Introducing $\lambda=\sqrt{\pi\rho_0}\,\tau$, $\tilde{\Omega}=\Omega/\sqrt{\pi\rho_0}$ and $\tilde{\Lambda}=\Lambda/\sqrt{\pi\rho_0}$, we rewrite Eqs. (2·21)~(2·25) as

$$\ddot{a}_1=a_1(\tilde{\Omega}^2+\tilde{\Lambda}^2)-2a_2\tilde{\Omega}\tilde{\Lambda}-2a_1A_1+\frac{2P_c}{\pi\rho_0{}^2a_1}-\frac{\tilde{C}_{11}}{\pi\rho_0}a_1\,, \tag{2·32}$$

$$\ddot{a}_2=a_2(\tilde{\Omega}^2+\tilde{\Lambda}^2)-2a_1\tilde{\Omega}\tilde{\Lambda}-2a_2A_2+\frac{2P_c}{\pi\rho_0{}^2a_2}-\frac{\tilde{C}_{22}}{\pi\rho_0}a_2\,, \tag{2·33}$$

$$\ddot{a}_3=-2a_3A_3+\frac{2P_c}{\pi\rho_0{}^2a_3}-\frac{\tilde{C}_{33}}{\pi\rho_0}a_3\,, \tag{2·34}$$

$$\dot{\tilde{b}}_1=-\dot{a}_1\tilde{\Lambda}+\dot{a}_2\tilde{\Omega}-\frac{\tilde{C}_{12}}{\pi\rho_0}a_2\,, \tag{2·35}$$

$$\dot{\tilde{b}}_2=\dot{a}_2\tilde{\Lambda}-\dot{a}_1\tilde{\Omega}-\frac{\tilde{C}_{21}}{\pi\rho_0}a_1\,, \tag{2·36}$$

where

$$\tilde{b}_1=a_1\tilde{\Lambda}-a_2\tilde{\Omega}\,, \tag{2·37}$$

$$\tilde{b}_2=-a_2\tilde{\Lambda}+a_1\tilde{\Omega}\,. \tag{2·38}$$

Hereafter "$\cdot$" denotes $\partial/\partial\lambda$. P_c is determined by the incompressible condition $\dot{\rho}=\ddot{\rho}$

$=0$ and written as

$$\frac{2P_c}{\pi\rho_0{}^2}=(\sum_{i=1}^{3}a_i{}^{-2})^{-1}\left[\sum_{i=1}^{3}\left(\frac{\dot{a}_i}{a_i}\right)^2-2(\tilde{\Omega}^2+\tilde{\Lambda}^2)+2\tilde{\Omega}\tilde{\Lambda}\left(\frac{a_2}{a_1}+\frac{a_1}{a_2}\right)+4\right]. \tag{2·39}$$

Finally, we define the energy, the angular momentum and the circulation of the internal motion of the fluid,[4]

$$E_{\rm int}=\frac{\pi\rho_0 m}{5}\left[\frac{1}{2}\sum_{i=1}^{3}\dot{a}_i{}^2+\frac{1}{2}(a_1{}^2+a_2{}^2)(\tilde{\Omega}^2+\tilde{\Lambda}^2)-2a_1a_2\tilde{\Omega}\tilde{\Lambda}-2A_0\right], \tag{2·40}$$

$$L_{\rm int}=\frac{m}{5}\{(a_1{}^2+a_2{}^2)\Omega-2a_1a_2\Lambda\}, \tag{2·41}$$

$$C_r=\pi a_1a_2\left(2\Omega-\Lambda\frac{a_1{}^2+a_2{}^2}{a_1a_2}\right). \tag{2·42}$$

If $E_{\rm int}<0$, the star is in a gravitationally bound state, but if $E_{\rm int}\geq 0$, it will be tidally disrupted. We note that $E_{\rm int}$ and $L_{\rm int}$ are not the conserved quantities when the tidal effects from the BH exist,[4] while C_r is the conserved quantity.

§ 3. Equilibrium configurations

In this section, we derive equilibrium configurations of the fluid star in circular orbits around a Kerr BH. In the case of equilibrium, $\dot{a}_i=\ddot{a}_i=\dot{b}_i=0$, $\alpha=\Psi=\sqrt{M/r_0{}^3}\,\tau$ and $\Omega=\sqrt{M/r_0{}^3}$. Thus, the following three equations determine the equilibrium state:

$$0=a_1{}^2\tilde{\Lambda}^2-2a_1a_2\tilde{\Omega}\tilde{\Lambda}-2a_1{}^2A_1+\frac{2P_c}{\pi\rho_0{}^2}+3a_1{}^2\tilde{\Omega}^2\frac{\Delta_0}{P_0}, \tag{3·1}$$

$$0=a_2{}^2\tilde{\Lambda}^2-2a_1a_2\tilde{\Omega}\tilde{\Lambda}-2a_2{}^2A_2+\frac{2P_c}{\pi\rho_0{}^2}, \tag{3·2}$$

$$0=-2a_3{}^2A_3+\frac{2P_c}{\pi\rho_0{}^2}-a_3{}^2\tilde{\Omega}^2\left(3\frac{\Delta_0}{P_0}-2\right). \tag{3·3}$$

If $\Lambda=0$, these equations reduce to those derived by Fishbone.[3] Note that for the case $\Psi=\alpha$, the 1-axis is tangent to the radial coordinates of Kerr.

Following Chandrasekhar,[7] we introduce

$$a_2=\frac{a_2}{a_1}, \tag{3·4}$$

$$a_3=\frac{a_3}{a_1}, \tag{3·5}$$

$$f\equiv\frac{a_1{}^2+a_2{}^2}{2a_1a_2}\frac{\Lambda}{\Omega}. \tag{3·6}$$

Then the circulation and the angular momentum of the fluid are written as

$$C_r=2\pi a_1a_2\Omega(1-f), \tag{3·7}$$

$$L_{\rm int}=\frac{1}{5}ma_1^2\Omega\left(1+\alpha_2^2-\frac{4\alpha_2^2}{1+\alpha_2^2}f\right). \tag{3·8}$$

Note that in the case when the viscosity of the fluid star is negligible, C_Γ conserves even if the dissipation due to gravitational waves exists. Thus, if the fluid star at a large separation from the BH does not have the spin angular momentum initially (i.e., $f=1$ and $\alpha_2=1$ at $r\gg M$), the circulation is zero throughout the whole evolution.

Eliminating $\tilde{\Omega}$ and P_c/ρ_0^2 from Eqs. (3·1)~(3·3), we get

$$\frac{A_1-\alpha_3^2A_3}{A_1-\alpha_2^2A_2}=\frac{4\alpha_2^2f^2/(1+\alpha_2^2)^2-4\alpha_2^2f/(1+\alpha_2^2)+3(1+\alpha_3^2)\Delta_0/P_0-2\alpha_3^2}{4\alpha_2^2(1-\alpha_2^2)f^2/(1+\alpha_2^2)^2+3\Delta_0/P_0}. \tag{3·9}$$

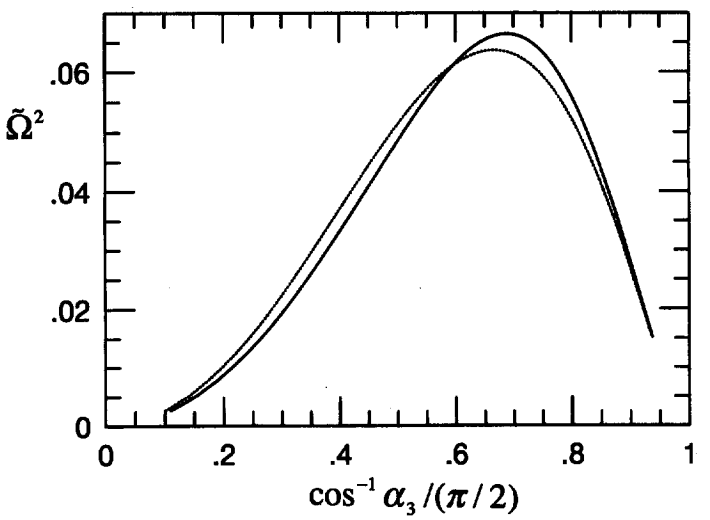

Fig. 1. $\tilde{\Omega}^2$ as a function of $\theta_3=\cos^{-1}\alpha_3/(\pi/2)$ at the ISCO for $f=0$(solid line) and $f=1$(dotted line).

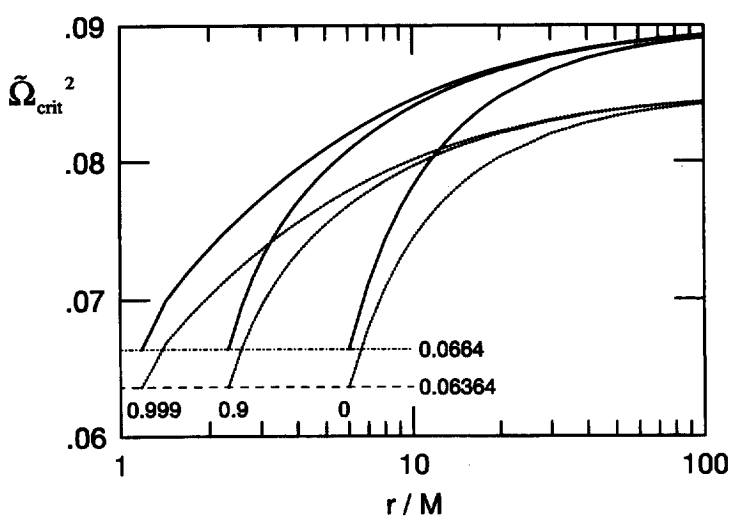

Fig. 2. $\Omega_{\rm crit}^2$ as a function of r_0 for $a/M=0$, 0.9, and 0.999 and for $f=0$(solid lines) and $f=1$(dotted lines).

Thus, the equilibrium configuration is obtained as follows: first, we fix f; then, once α_2 is given, α_3 is determined from Eq. (3·9). When α_2 and α_3 are determined, $\tilde{\Omega}$ is calculated from

$$\tilde{\Omega}^2=2(A_1-\alpha_2^2A_2)\left\{3\frac{\Delta_0}{P_0}+\frac{4f^2\alpha_2^2}{(1+\alpha_2^2)^2}(1-\alpha_2^2)\right\}^{-1}. \tag{3·10}$$

First of all, in Fig. 1, we show the variation of $\tilde{\Omega}^2$ as a function of $\theta_3\equiv\cos^{-1}\alpha_3/(\pi/2)$ at the ISCO for $f=0$ (i.e., the Roche ellipsoid; solid line) and $f=1$ (i.e., the IRRE; dotted line). Although the maximum value of $\tilde{\Omega}^2$ is changed by the relativistic correction and the internal motion of the fluid star, the shapes of the

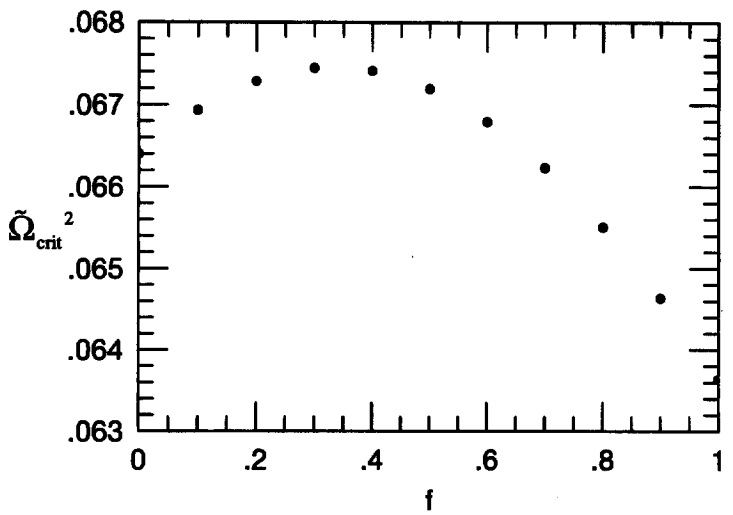

(a)

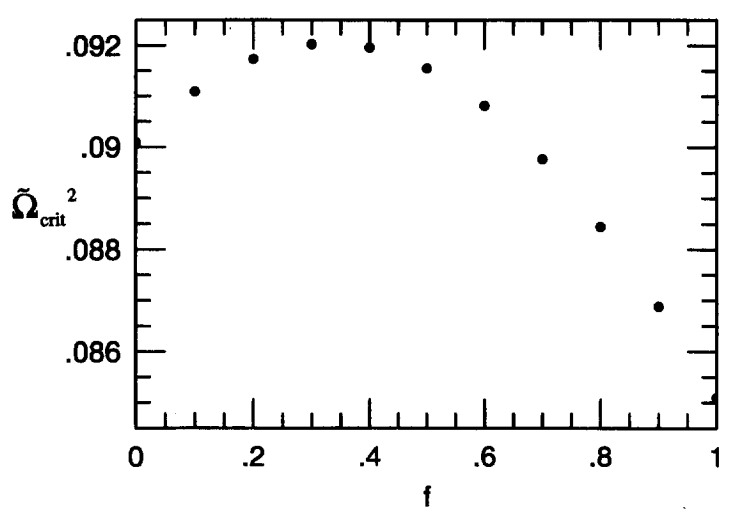

(b)

Fig. 3. Ω_{crit}^2 as a function of f at the ISCO(a) and at infinity(b).

function $\tilde{\Omega}(\theta_3)^2$ are regarded as the typical one for Roche and Roche-Riemann sequences irrespective of the relativistic effect; i.e., $\tilde{\Omega}$ has a maximum $\tilde{\Omega}^2_{\rm crit}$ at $\theta_3 \sim 0.6 - 0.7$. Hereafter, we call the configurations at $\tilde{\Omega}=\tilde{\Omega}_{\rm crit}$ the Roche or Roche-Riemann limits. In Fig. 2, we show $\tilde{\Omega}^2_{\rm crit}$ at a given r_0 as a function of r_0/M for $a/M=0$, 0.9 and 0.999. For these BHs, the radii of the ISCO, $r_{\rm ISCO}$, are $6M$, $\simeq 2.32M$ and $\simeq 1.18M$, respectively. Solid lines denote the cases $f=0$, and dashed lines denote the cases $f=1$. At the ISCO, $\tilde{\Omega}^2_{\rm crit} \simeq 0.066399$ for $f=0$[3] and $\simeq 0.063637$ for $f=1$. Note that, at infinity, i.e., in the Newtonian limit, it becomes $\simeq 0.09009$ for $f=0$ and $\simeq 0.08509$ for $f=1$.[7),8)] In Fig. 3, we show $\tilde{\Omega}^2_{\rm crit}$ at the ISCO (a) and at infinity (b) as a function of f. It is found that due to the relativistic correction, $\tilde{\Omega}_{\rm crit}$ decreases about 15 %, but the effect of the circulation is small.

In Fig. 4, we show α_2 and α_3 at $\tilde{\Omega}=\tilde{\Omega}_{\rm crit}$ as a function of f, respectively. Solid and dotted lines denote α_2 and α_3 at the ISCO, and dashed and long-dashed lines denote α_2 and α_3 at infinity. A general feature is that irrespective of the general relativistic effect, for the Roche ellipsoid, α_2 is always greater than α_3 at the Roche limit, and for the IRRE, α_3 is always greater than α_2 at the Roche-Riemann limit. In any case, if α_2 becomes smaller than $\sim 0.48-0.51$, the incompressible fluid star will reach the Roche-Riemann limit.

In Figs. 5 and 6, we show sequences of the IRRE as a function of r_0 for $a=0$ (Fig. 5) and $0.9M$ (Fig. 6). For each a, we show (a)$\tilde{\Omega}^2$, (b)α_2, (c)$E_{\rm int}$ and (d)$L_{\rm int}$, where the units of $E_{\rm int}$ and $L_{\rm int}$ are m^2/R_0 and $m^{3/2}R_0^{1/2}$, respectively. In each figure, ρ_0 is chosen to satisfy $\tilde{\Omega}=\tilde{\Omega}_{\rm crit}$ at the ISCO (solid lines), $\tilde{\Omega}=\tilde{\Omega}_{\rm crit}$ at $r_0=r_{\rm ISCO}+0.5M$ (dashed lines), and $\tilde{\Omega}=\tilde{\Omega}_{\rm crit}/\sqrt{2}$ at the ISCO (dotted lines). If the orbital radius of the fluid star is assumed to decrease only due to the emission of gravitational waves, these lines may be regarded as the evolution sequences. From figures, we can see that α_2, $E_{\rm int}$ and $L_{\rm int}$ rapidly change only near the Roche-Riemann limit. Since the models indicated by dotted lines do not reach the Roche-Riemann limit at the ISCO, these quantities

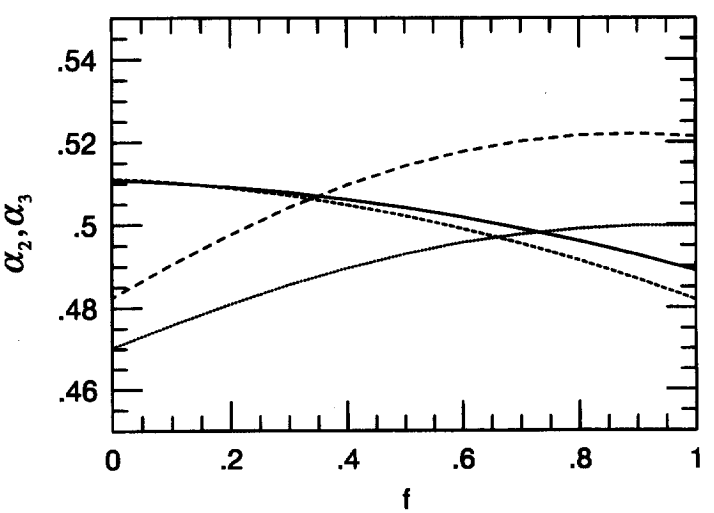

Fig. 4. α_2 and α_3 as a function of f. Solid and dotted lines donote α_2 and α_3 at the ISCO, and dashed and long-dashed lines denote α_2 and α_3 at infinity.

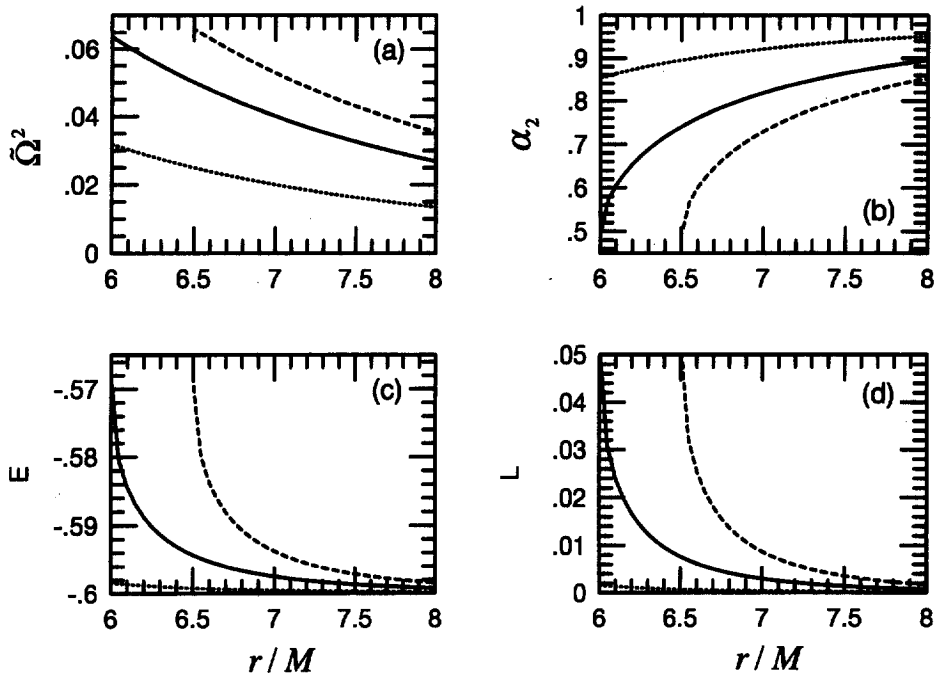

Fig. 5. (a)$\tilde{\Omega}^2$, (b)α_2, (c)$E_{\rm int}$ and (d)$L_{\rm int}$ as a function of r_0 for sequences of the IRRE and for $a=0$. Here, the units of $E_{\rm int}$ and $L_{\rm int}$ are m^2/R_0 and $m^{3/2}R_0^{1/2}$, respectively. ρ_0 is chosen to satisfy $\tilde{\Omega}=\tilde{\Omega}_{\rm crit}$ at $r_0=r_{\rm isco}$(solid line), $\tilde{\Omega}=\tilde{\Omega}_{\rm crit}$ at $r_0=r_{\rm isco}+0.5\,M$(dashed line), and $\tilde{\Omega}=\tilde{\Omega}_{\rm crit}/\sqrt{2}$ at $r_0=r_{\rm isco}$(dotted line), respectively.

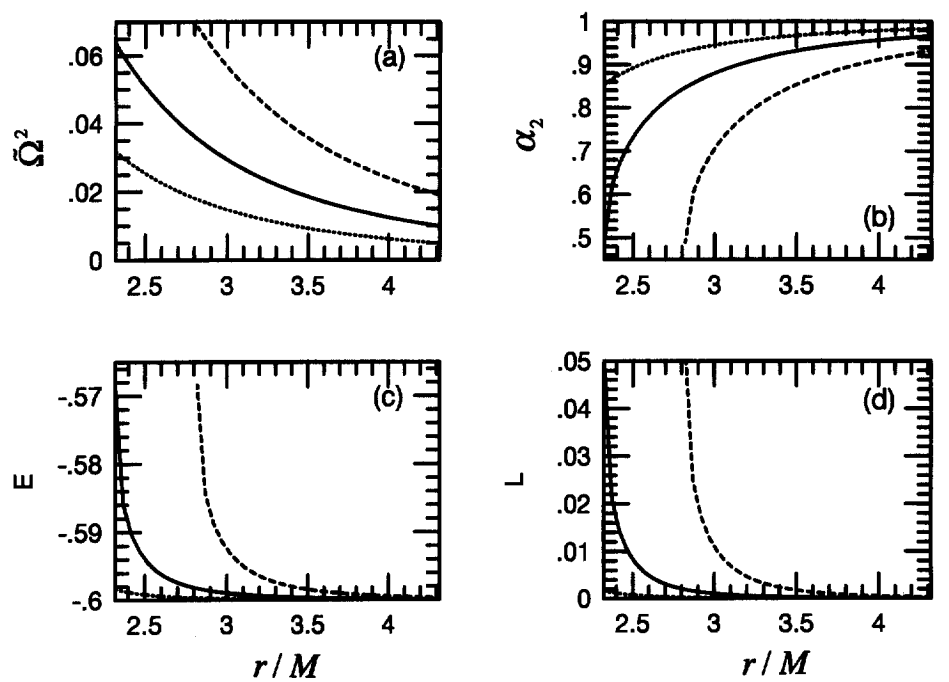

Fig. 6. The same as Fig. 5, but for $a=0.9\,M$.

only mildly change throughout the whole sequence. This is trivial because in such a binary, the density of the fluid star is high enough that the tidal effect can be safely neglected and the star is approximately regarded as a spherical one.

§ 4. Time evolution of equilibrium configurations

In this section, we investigate the dynamical stability and the fate of the dynamically unstable star integrating dynamical equations. The basic equations are Eqs. (2·32)~(2·36),

$$\dot{\Psi}=\sqrt{\frac{M}{\pi\rho_0 r_0^3}} \quad \text{and} \quad \dot{\alpha}=\tilde{\Omega}\,. \tag{4·1}$$

Note that the orbit of the fluid star is fixed as a geodesic circular orbit. In the case of circular orbits, $\Psi-\alpha$ may be regarded as a misalignment angle between the axis a_1 of the ellipsoid and the line joining the centers of the BH and the fluid star.

We numerically integrate these equations forward in time using a fourth-order Runge-Kutta method.[9] As initial conditions, we adopt equilibrium solutions obtained in § 3 except for a small perturbation as

$$\dot{a}_1=\eta a_1\,, \quad \dot{a}_2=-\eta a_2 \tag{4·2}$$

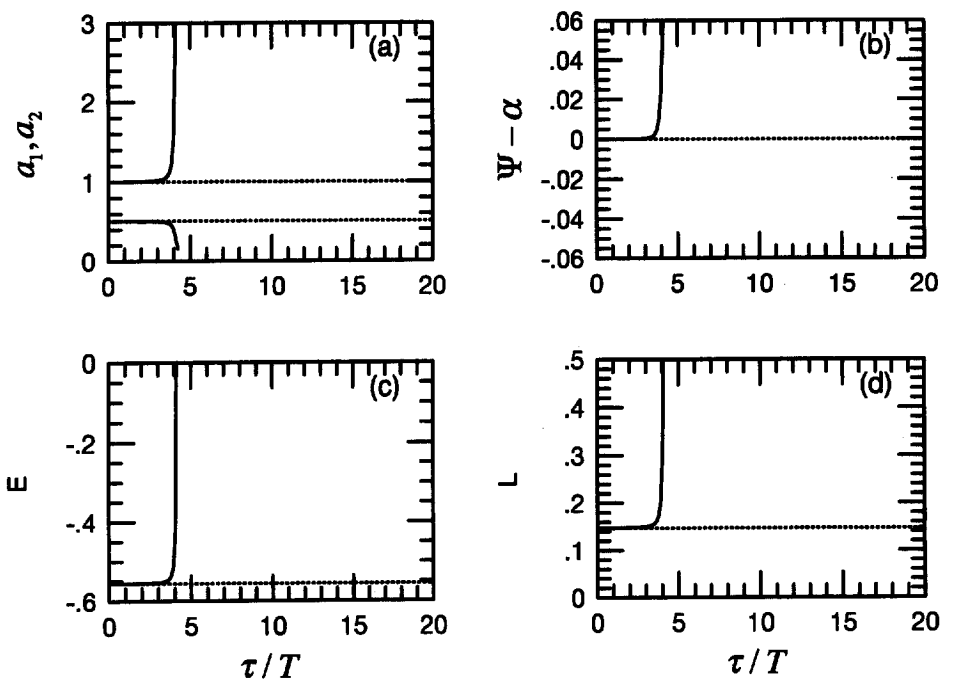

Fig. 7. Time evolutions of Roche-Riemann ellipsoids with s small perturbation shown in Eq. (4·2). We show (a)$a_1(t)/a_1(0)$ and $a_2(t)/a_1(0)$; (b)$(\Psi-\alpha)/(2\pi)$; (c)$E_{\rm int}/(m^2/R_0)$; (d)$L_{\rm int}/(m^{3/2}R_0^{1/2})$. The units of the time($\tau$) is T. As initial conditions, the Roche ellipsoid at $r_0=r_{\rm isco}$ with $a_2=0.5050$(solid lines) and $a_2=0.5070$(dotted lines) are used.

or

$$\tilde{\Omega}^2=\tilde{\Omega}_{\rm crit}^2(1+\xi)\,, \tag{4·3}$$

where η and ξ are small parameters. We set η as 10^{-4}. It is noted that we adopted other types of perturbations instead of the above, but we obtained the same results concerning the stability. In time evolutions, we have two constraints; one is that $\dot{\rho}_0=0$, thus, $a_1a_2a_3=R_0^3$=constant, and the other is conservation of the circulation C_Γ. We find that in numerical calculations, two constants of motion are kept constant with sufficient accuracy.

Hereafter, in figures, we show time evolutions of (a) $a_1(t)/a_1(0)$ and $a_2(t)/a_1(0)$, (b) $(\Psi-\alpha)/(2\pi)$, (c) $E_{\rm int}/(m^2/R_0)$ and (d) $L_{\rm int}/(m^{3/2}R_0^{1/2})$. The units of time($\tau$) are $T\equiv 2\pi\sqrt{r_0^3/M}$. We choose the orbital radius as $r_0=r_{\rm ISCO}$ in all cases.

First, we consider time evolutions of relativistic Roche ellipsoids. The dynamical stability of them was investigated in the second paper of Fishbone.[3] He found that the instability sets in for a configuration somewhat more distorted than the Roche-limit configuration; for $r_0=r_{\rm ISCO}$, $\alpha_2\simeq 0.5110$ at the Roche limit, while the dynamical instability sets in at $\alpha_2\simeq 0.5051$.[3] This implies that a Roche ellipsoid is dynamically stable even if it is more deformed than the Roche-limit ellipsoid. In Fig. 7, we show numerical results of the time evolution from the initial configurations with $\alpha_2=0.5050$ (solid lines) and $\alpha_2=0.5070$ (dotted lines). As mentioned above, the former is the unstable configuration and the latter is the stable one, and the numerical

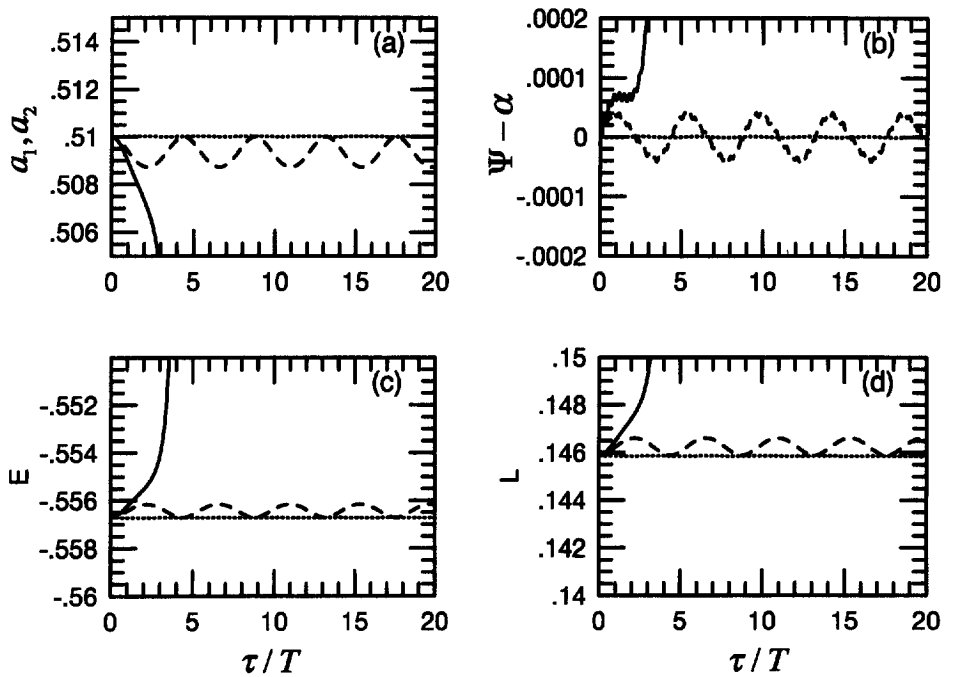

Fig. 8. The same as Fig. 7, but numerical results shown are those started from different initial conditions. As initial conditions, we use the Roche ellipsoid at $r_0=r_{\rm ISCO}$ with $\alpha_2=0.5100$ including a small perturbation in $\tilde{\Omega}$(see text). Note that in Fig. 8(a), we only show $a_2(t)/a_1(0)$.

results demonstrate those facts. For the unstable ellipsoid, a_1 and $\Psi - \alpha$ become larger and larger, and a_2 and a_3 become smaller and smaller. Thus, the configuration of the ellipsoid becomes spindle-like one with time evolution, and direction of the major axis of the spindle also deviates from the radial direction. For $\tau > 4T$, $E_{\rm int}$ becomes positive. This implies that at that time the ellipsoid is tidally disrupted.

In Fig. 8, we show the time evolution of the Roche ellipsoid started from initial configurations with $a_2 = 0.5100$ including the perturbation shown in Eq. (4·3). (In Fig. 8(a), we only show $a_2(t)/a_1(0)$.) Solid, dotted and dashed lines denote the cases $\xi = 5\times10^{-4}$, $\xi = 3\times10^{-4}$ and $\xi = 0$. In these cases, we do not add the perturbation shown in Eq. (4·2). For $\xi = 0$, the configuration is stable, and it is also demonstrated in the numerical calculation. For $\xi = 3\times10^{-4}$ and $\xi = 5\times10^{-4}$, $\tilde{\Omega}$ is over $\tilde{\Omega}_{\rm crit}$ in either case, but their fates are different; for the former case, the ellipsoid is stable and purely oscillating, while for the latter case, the ellipsoid is unstable and soon tidally disrupted. Thus, for the Roche ellipsoid beyond the Roche limit, the stability analysis seems useless. Instead, we need a stability analysis for oscillating ellipsoids, and results shown in Fig. 8 suggest the following conclusion: If an incompressible star reaches the Roche limit, it is stable. However, if the orbital radius slightly shrinks due to a mechanism such as emission of gravitational waves, the Roche ellipsoid changes to an oscillating state. However, it will soon become unstable for a further shrink of the orbital radius before it reaches the dynamical instability point for the Roche ellipsoid, $a_2 \simeq 0.5051$.

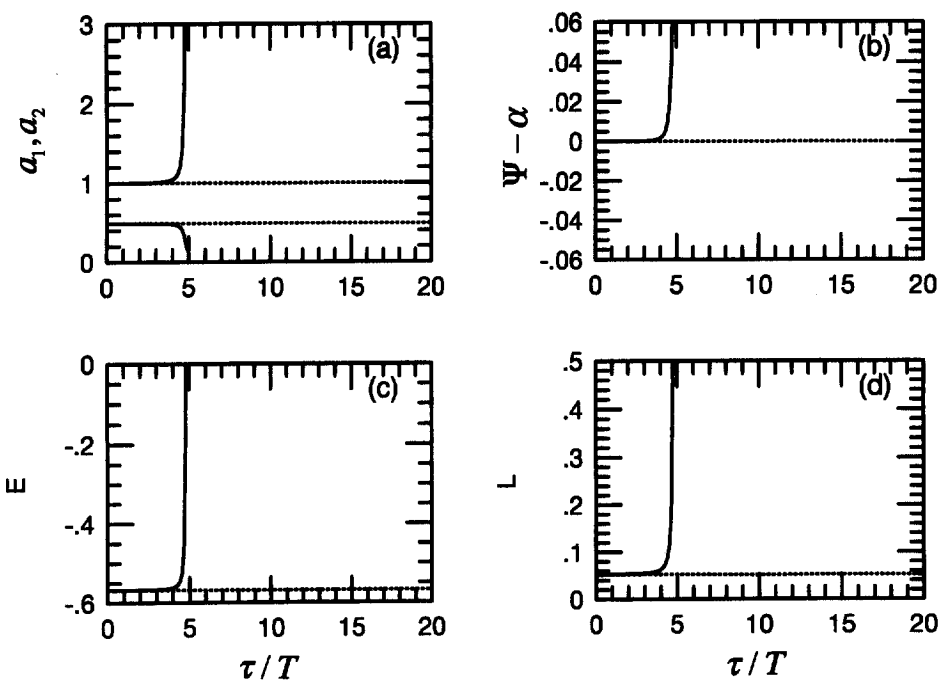

Fig. 9. The same as Fig. 7, but numerical results shown are those started from different initial conditions. As initial conditions, we use the IRREs at $r_0 = r_{\rm isco}$ with $a_2 = 0.4880$(solid lines), and $a_2 = 0.4900$(dotted lines) including a small perturbation shown in Eq. (4·2).

Then, we consider the stability of relativistic IRREs which are likely realized for BH-NS binaries.[6] As initial conditions, we adopt the configuration beyond the Roche-Riemann limit ($a_2=0.4880$), and slightly different, but tidally stable state $a_2=0.4900$. In either case, $\tilde{\Omega}^2\simeq 0.063637$. Note that at the Roche-Riemann limit, $a_2\simeq 0.48895$ and $\tilde{\Omega}^2\simeq 0.063637$. In Fig. 9, we show numerical results: Solid and dotted lines denote time evolutions for configurations of $a_2=0.4880$ and 0.4900, respectively, and we find that the former is dynamically unstable and the latter is stable. The numerical results indicate that the point where the dynamical instability sets in is very near the Roche-Riemann limit for the IRRE. This has also been pointed out for Newtonian case previously.[8] Thus, for the IRRE, the dynamical stability limit will be almost equal to the Roche-Riemann limit.

Finally, we note the following fact; at the time of the tidal disruption, $L_{\rm int}$ becomes about ten times of the initial value getting the tidal torque from the BH. According to the theory of accretion disks around BHs, the final fate of the accreting fluid will critically depend on the angular momentum.[10] Thus, the gain of the angular momentum by the tidal torque may play an important role for subsequent evolution of the fluid.

§ 5. Discussion

In § 3, we find that for the IRRE, $\tilde{\Omega}^2_{\rm crit}\geq 0.063637$ holds, where the minimum value is taken at the ISCO. Thus, if the density of a fluid star is larger than $M/(0.063637\pi r^3_{\rm ISCO})$, the star is never tidally disrupted. Let us apply this result to BH-NS binary systems in order to derive a rough value of the tidal disruption limit for NSs. According to the above estimate, a NS is tidally disrupted by a BH if the mass of the BH satisfies the following condition:

$$M\leq m\left(\frac{4}{3\times 0.063637}\right)^{1/2}\left(\frac{M}{r_0}\right)^{3/2}\left(\frac{R_0}{m}\right)^{3/2}=4.64M_\odot\left(\frac{1.4M_\odot}{m}\right)^{1/2}\left(\frac{R_0}{10\ {\rm km}}\right)^{3/2}\left(\frac{6M}{r_0}\right)^{3/2}, \tag{5·1}$$

where $M_\odot$ denotes the solar mass. Thus, if we assume that typical mass and radius of NSs are $1.4M_\odot$ and 10 km, respectively, it will be tidally disrupted by a Schwarzschild BH of mass$<4.64M_\odot$, by a Kerr BH of spin $a=0.9M$ and mass$<19.3M_\odot$ and by the extreme Kerr BH($a=M$) of mass$<68.2M_\odot$. We note that the difference of the maximum value of BH mass simply comes from the fact that the radius of ISCO is smaller for larger spin parameter of Kerr BH. Since the approach in this paper can be applied to the binary systems which satisfy $M\gg m$, these are very rough estimates for the tidal disruption limit. But, it will be a guideline to a correct estimate.

Finally, we comment on the deviation of the ISCO for the IRRE due to the quadrupole moment of the fluid star induced by the tidal force of the BH. The total energy of the system is approximately written as

$$E_{\rm tot}(r_0)=E(r_0)+E_{\rm int}(r_0)+E_{\rm quad}(r_0)\,, \tag{5·2}$$

where $E_{\rm quad}$ is the correction by the quadrupole moment of the fluid star, which changes the orbital velocity of the star and the orbital binding energy between the BH

and the star. The ISCO is determined from

$$\frac{dE_{\rm tot}}{dr_0}=0\,. \tag{5·3}$$

dE/dr_0 satisfies

$$\frac{dE}{dr_0}\begin{cases}>0 & \text{for} \quad r_0>r_{\rm ISCO}\,,\\ <0 & \text{for} \quad r_0<r_{\rm ISCO}\,.\end{cases} \tag{5·4}$$

In this paper, we find $dE_{\rm Int}/dr_0<0$ throughout the whole sequences of the IRRE. On the other hand, we do not know how to estimate $E_{\rm quad}$ accurately up to now. To see an order of magnitude of $E_{\rm quad}$, we use the Newtonian formula[8] which holds only for $r_0\gg M$,

$$E_{\rm quad}=\frac{Mm}{20r_0^3}(2a_1{}^2-a_2{}^2-a_3{}^2)\,. \tag{5·5}$$

In this formula, $dE_{\rm quad}/dr_0<0$. Therefore, both $E_{\rm Int}$ and $E_{\rm quad}$ contribute to increase the radius of the ISCO. Note that the order of magnitude of $dE_{\rm Int}/dr_0$ is $\sim R_0m^2/r_0^3$ and that of $dE_{\rm quad}/dr_0$ is $\sim R_0{}^2mM/r_0^4$. In the BH-NS binary, $M/r_0\sim m/R_0$ near the ISCO, so that $|dE_{\rm Int}/dr_0|\sim|dE_{\rm quad}/dr_0|$ there. Thus, to evaluate the deviation of the ISCO accurately, the accurate formula for $E_{\rm quad}$ is necessary. A present rough estimate shows, however, that the tidal effect seems to make the radius of the ISCO larger by order $(R_0/r_0)^2\sim(R_0/r_0)(m/M)$, which is not a negligible factor to determine the correct ISCO as pointed out by Lai et al.[8] and other recent works.[11)~13)]

Acknowledgements

The author thanks H. Asada, Y. Mino, M. Sasaki and T. Tanaka for discussions. This work was in part supported by a Grant-in-Aid of the Ministry of Education, Culture, Science and Sports (No. 08237210).

References

1) A. Abramovici et al., Science **256** (1992), 325.
K. S. Thorne, in *Proceedings of the 8th Nishinomiya-Yukawa Memorial Symposium on Relativistic Cosmology*, ed. M. Sasaki (Universal Academy Press, Tokyo, 1994), p. 67.
2) R. Narayan, B. Paczynski and T. Piran, Astrophys. J. **395** (1992), L83.
P. Meszaros and M. J. Rees, Astrophys. J. **397** (1992), 570; Astro-ph 9609065, submitted to Astrophys. Lett.; as for their works, see references cited therein.
G. J. Fishman and C. A. Meegan, Ann. Rev. Astron. Astrophys. **33** (1995), 415, and references cited therein.
3) L. G. Fishbone, Astrophys. J. **185** (1972), 43; **195** (1975), 499.
4) B. Mashhoon, Astrophys. J. **197** (1975), 705.
5) J.-A. Marck, Proc. R. Soc. London **A385** (1983), 431.
J.-P. Luminet and J.-A. Marck, Mon. Not. R. Astron. Soc. **212** (1985), 57.
6) C. S. Kochanek, Astrophys. J. **398** (1992), 234.
L. Bildsten and C. Cutler, Astrophys. J. **400** (1992), 175.
7) S. Chandrasekhar, *Ellipsoidal Figures of Equilibrium* (Dover, 1987).
8) D. Lai, F. A. Rasio and S. L. Shapiro, Astrophys. J. Supple. **88** (1993), 205.
9) W. H. Press, B. P. Flannery, S. A. Teukolsky and W. T. Vetterling, *Numerical Recipies* (Cambridge University Press, 1992).

10) M. Abramowicz, M. Jaroszynski and M. Sikora, Astro. Astrophys. **63** (1978), 221.
11) D. Lai and A. G. Wiseman, Phys. Rev. **D54** (1996), 3958.
12) W. Ogawaguchi and Y. Kojima, Prog. Theor. Phys. **96** (1996), 901.
13) K. Taniguchi and T. Nakamura, Prog. Theor. Phys. **96** (1996), 693.